J. Am. Soc. Mass Spectrom. (2018) 29:2305–2316
DOI: 10.1007/s13361-018-2048-1

RESEARCH ARTICLE

Analysis of the Thermal Stability of Very Thin Surface Layers of Corrosion Inhibitors by Time-of-Flight Secondary Ion Mass Spectrometry

Janez Kovač,[1] Matjaž Finšgar[2]

[1]Department of Surface Engineering and Optoelectronics, Jozef Stefan Institute, Jamova 39, 1000, Ljubljana, Slovenia
[2]Faculty of Chemistry and Chemical Engineering, University of Maribor, Smetanova ulica 17, 2000, Maribor, Slovenia

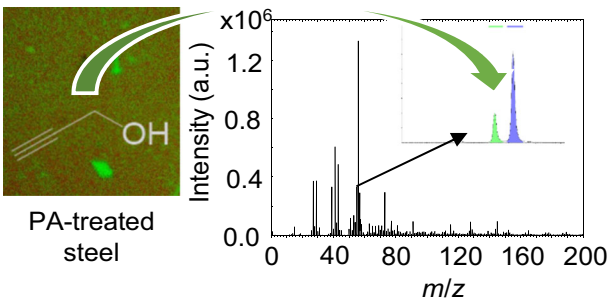

Abstract. The powerful nature of the secondary ion mass spectrometry (SIMS) technique was explored in order to analyse very thin surface layers that were self-assembled on steel material from acidic solution. These surface layers are adsorbed corrosion inhibitors. The SIMS technique proved useful to characterise the molecular structure and homogeneity of thin surface layers in the nanometre range of specific analytes on the metallic substrate. Using SIMS, the thermal stability of these layers was further investigated and the desorption energy at a certain temperature was determined, where special attention was devoted to the method's static limit. In order to compare, and for certain cases emphasise, the benefits gained by using SIMS in such surface analysis compared with the X-ray photoelectron spectroscopy (XPS) method, the same samples were also analysed by means of the latter. XPS is usually considered to be the most powerful analytical tool in surface analysis studies, but, as shown herein, it has certain limitations compared to SIMS. Finally, the surface topography was investigated by employing atomic force microscopy (AFM) in order to carry out a comprehensive surface analysis.

Keywords: Secondary ion mass spectrometry, SIMS, Surface analysis, Thermal stability, Desorption energy, Propargyl alcohol, Cinnamaldehyde

Received: 14 February 2018/Revised: 2 August 2018/Accepted: 2 August 2018/Published Online: 17 August 2018

Introduction

In order to identify and reveal the manner of substrate-adsorbate bonding, where a low amount of adsorbate is present in the analytical sense, surface analytical techniques are of paramount importance. X-ray photoelectron spectroscopy (XPS) is probably the most widely employed surface analytical technique in the surface analysis of corrosion inhibitors [1]. Lately, with the development of the secondary ion mass spectroscopy (SIMS) technique, additional information on chemical bonding at the metal–adsorbate interface can be obtained. As will be shown herein, the SIMS technique can be used to study the thermal degradability of the surface layers more effectively than by XPS, which is especially important in oilfield application where elevated temperatures are encountered (i.e. 150 °C or even higher). The SIMS method has very high chemical selectivity combined with high lateral resolution, surface sensitivity and a relatively low detection limit. The method is based on the bombardment of the sample surface with a focused ion beam of energy of 30 keV and the subsequent desorption of neutral atoms and molecules as well as ionised particles such as ions, molecules or molecular fragments. The limitation of the SIMS method is the quantification of the surface composition since the ionisation probability of forming secondary ions greatly depends on the electronic state of the surface, which is known as a matrix effect [2–4]. It has to be emphasised that the SIMS method has not been frequently employed as a surface analytical technique for studying the adsorption of corrosion inhibitors. A few examples can be found in [2, 5–8].

A corrosion inhibitor is a chemical compound that is added in very small amounts (frequently 1 wt% and max. up to 3 wt%) to a specific environment that is corrosive for metals

Correspondence to: Matjaž Finšgar; *e-mail:* matjaz.finsgar@um.si

or alloys [9]. Then, the corrosion inhibitor adsorbs in a certain manner on the metal or alloy surface and starts to mitigate corrosion. Most of the current corrosion inhibitors are organic compounds having N, O or S atoms and/or an aromatic character in their structures. In most cases, how the corrosion inhibitor works is not known. Empirical tests are usually performed to prove that a particular molecule works or not for a specific metallic material in a certain environment. However, with knowledge of the manner of corrosion inhibitor bonding to the surface, it is possible to determine which parts of a particular molecule are crucial for the corrosion inhibition effect. Therefore, knowledge of this phenomenon can enable the design of new compounds that effectively protect metallic materials (possibly environmentally more acceptable compounds in order to reduce, e.g. toxicity, which is frequently a major problem when employing corrosion inhibitors [9]). Moreover, once such data is obtained, corrosion inhibitor design can also be focused on the development of newly synthesised universal corrosion inhibitors to protect various metallic materials in different environments simultaneously.

The main emphasis of this work is to show the powerful nature of the SIMS technique to study very thin layers (1–5 nm) on a steel surface, which can provide crucial information that cannot be obtained with the XPS method. Standard corrosion inhibitors, propargyl alcohol (PA) and cinnamaldehyde (CIN), adsorbed on a steel surface were selected for this model study. PA and CIN were selected as the model corrosion inhibitors as these compounds are known to be effective corrosion inhibitors for lower-grade steel materials in acidising oilfield applications [9–19]. The structures of the adsorbed compounds on the C15 steel surface are given in Figure 1. C15 steel is a low-carbon steel and represents a metallic material for which 15 wt% HCl (employed in this study) is highly corrosive and which needs to be protected by, e.g. the CIN or PA corrosion inhibitors employed herein [9]. A concentration of 15 wt% HCl and 1 wt% of corrosion inhibitor was employed in this study to perform the adsorption of the corrosion inhibitors. These concentrations are considered to be standard concentrations in oilfield application [9]. The immersion of the sample for 1 h employed herein was also shown previously to be sufficient in the study of very thin surface layers of corrosion inhibitors [20]. Longer-term immersion periods could lead to the formation of too thick surface layers (more than 5 nm), which makes surface analysis difficult (especially by XPS).

It will be shown that the SIMS technique is a more useful surface analytical technique than XPS for such studies. In particular, SIMS was crucial for obtaining more certain proof that these relatively simple organic compounds were actually adsorbed on the surface. It will be also shown that by using SIMS, it is possible to investigate when the molecules desorb from the surface due to a temperature increase. Moreover, SIMS also provides better microscopic surface imaging compared to XPS. To the best of the authors' knowledge, no such study has hitherto been performed.

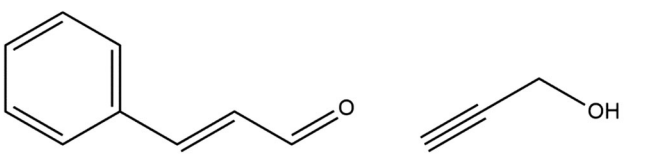

Figure 1. Structures of molecules that formed self-assembled surface layers on the C15 steel

Experimental

ToF-SIMS

Time-of-flight (ToF)-SIMS analyses were performed using a ToF-SIMS 5 instrument (ION-TOF, Münster, Germany) equipped with a bismuth liquid metal ion gun with a kinetic energy of 30 keV. The analyses were performed in an ultra-high vacuum of approximately 10^{-7} Pa. The SIMS spectra were measured by scanning a Bi_3^+ cluster ion beam over areas 200×200 μm^2 in size. The beam current was 0.6 pA, and the total measuring time to acquire the SIMS spectra was 30 s. The dose of the primary ions during the measurements was in the static regime. The SIMS spectra were processed with SurfaceLab 6.7 (ION TOF) software. The positive secondary ion mass spectra were calibrated using CH_3^+ (mass to charge ratio m/z 15.02), $C_2H_3^+$ (m/z 27.02) and $C_2H_5^+$ (m/z 29.04), and the negative mass spectra were calibrated using C^- (12.00), C_2^- (m/z 24.00) and C_2H^- (m/z 25.01). The mass resolution $m/\Delta m$ during the SIMS measurements was approx. 10,000. The images of the total and selected secondary ions were acquired with a Bi_3^+ primary ion beam over a 450×450-μm^2 area with a 256×256-pixel resolution. The images were acquired over 3 min. An electron gun was used for charge compensation on the sample surfaces during the analysis. During thermal treatment, the analysed area was permanently changed across the sample's surface in order to avoid surface sputtering and to overcome the static limit that determines the surface sensitivity of the SIMS method. During sample annealing, the temperature was increased every 3 min by 15° (heating rate 5 K/min).

XPS and AFM Measurements

XPS analyses were carried out on a PHI-TFA XPS spectrometer produced by Physical Electronics Inc. The analysed area was 0.4 mm in diameter, and the analysed depth was approx. 3–5 nm. This high surface sensitivity is a general characteristic of the XPS method. Sample surfaces were excited by X-ray radiation from a monochromatic Al source with a photon energy of 1486.6 eV. The high-energy resolution spectra were acquired with an energy analyser operating at a resolution of approx. 0.6 eV and a pass energy of 29.3 eV. During data processing, the spectra were corrected by setting the C 1s peak to 284.8 eV, which is characteristic of C–C/C–H bonds. The accuracy of the binding energies was approx. ± 0.3 eV, and it is a measure of an uncertainty of the binding energy of XPS spectra influenced by instability and energy calibration of the electron energy analyser. The XPS data were processed with MultiPak software

(version 8.1c). For surface morphology investigations, a Solver PRO 45 atomic force microscope (AFM) instrument was employed (NT-MDT). The AFM measurements were performed in non-contact mode since the weakly bounded layer of organic inhibitors was expected on the surface.

Solutions and Material Preparation

C15 grade mild steel plates were supplied by Rocholl, Aglasterhausen, Germany (composition given in Table 1). Specimens for surface analysis were cut from the C15 material in the shape of discs 15 mm in diameter. These samples were ground under a stream of water with SiC papers (Struers, Ballerup, Denmark) using a rotating device. The grinding procedure started with 320-grid SiC papers, followed by 500-, 1000-, 1200-, 2400- and 4000-grid SiC papers in sequence. The grinding direction was changed four times by turning the sample 90° for each SiC paper to minimise abrasion. Afterwards, samples were thoroughly rinsed with ultrapure water, cleaned for 5 min in an ultrasound bath (50 wt% ultrapure water, 50 wt% EtOH) and dried under a stream of Ar. Ultrapure water, with a resistivity of 18.2 MΩ cm, was obtained from Milli-Q, Millipore Corporation (MA, USA).

In order to form surface layers of self-assembled PA or CIN, the prepared C15 steel samples were immersed for 1 h in 15 wt% HCl solution containing 1 wt% PA (purity of 99 wt%) or CIN (purity ≥ 99 wt%). PA and CIN were provided by Sigma Aldrich (St. Louis, MO, USA). Afterwards, these samples were washed with ultrapure water and dried under a stream of Ar.

All solutions were prepared with ultrapure water (with a resistivity of 18.2 MΩ cm) obtained from Milli-Q (Millipore Corporation, MA, USA).

The *m/z* of a CIN (C_9H_8O) molecule is 132.06 and that of a PA (C_3H_4O) molecule is 56.03. The relatively simple molecular structure and low molecular mass of both corrosion inhibitors mean that we could not expect signals in the ToF-SIMS spectra in the middle (*m/z* at 100–500) and high (above *m/z* 500) range, which was confirmed during measurements. The ToF-SIMS method in a *m/z* range above *m/z* 150 is usually the most useful due to the absence of hydrocarbon signals C_xH_y from fragments of organic molecules and possibly from adventitious carbon-containing molecules adsorbed on the steel surface from the atmosphere. Due to this reason, the detection of low-mass molecules was challenging, as shown below.

Results and Discussion

In order to exclude possible spectroscopic interferences by overlapping signals originating from contamination and adsorbed corrosion inhibitors, SIMS analyses were also performed on the C15 sample before (prepared ground sample) and after immersion in 15 wt% HCl solution (without PA and CIN). The adsorption of adventitious carbon species from the surrounding atmosphere is common for the metallic materials and may interfere such analysis [21–25]. However, characteristic signals that are reported below for the CIN and PA molecules were not present for sample after its preparation and after its immersion in 15 wt% HCl.

Table 1. The composition of the C15 grade mild steel plates as specified by the supplier

Element	C	Si	Mn	P	S	Fe
wt%	0.140	0.200	0.470	0.006	0.003	Balance

ToF-SIMS Results

Chemical Structure of the Adsorbed CIN Surface Layer Figure 2a shows a positive ion SIMS spectrum in the *m*/z range of 0–200 obtained from the CIN layer that was adsorbed on the C15 steel. The spectrum consists of many $C_xH_y^+$ related peaks. Three peaks at *m/z* 131.05, 132.06 and 133.07 are characteristic of CIN. The most intensive peak among them is located at *m/z* 131.05 representing a $C_9H_7O^+$ ion, i.e. $(M–H)^+$ [26] (the $(M–H)^+$ means the molecular ion $M^{+\cdot}$ after removal of one hydrogen radical, and the ion $(M+H)^+$ means the protonated molecule) [27]. The latter shows direct evidence of the presence of CIN molecules on the surface [28]. Other peaks closely related to the CIN molecules that were formed after ionisation and some rearrangements are at *m/z* 43.02 ($C_2H_3O^+$), 55.02 ($C_3H_3O^+$), 77.04 ($C_6H_5^+$), 91.05 ($C_7H_7^+$=C_6H_5–CH_2^+), 105.03 ($C_7H_5O^+$), 105.07 ($C_8H_9^+$) and 115.05 ($C_9H_7^+$). Furthermore, additional signals that correspond to hydrocarbon species were detected at *m/z* 27.02 ($C_2H_3^+$), 29.04 ($C_2H_5^+$), 41.04 ($C_3H_5^+$), 55.05 ($C_4H_7^+$) and 57.07 ($C_4H_9^+$) (possibly also at *m/z* 43.09 ($C_3H_7^+$)). These hydrocarbons most likely adsorbed during the preparation procedure of the steel sample, when it was dried and transferred to the spectrometer [24, 25, 29, 30]. In addition to hydrocarbons, Figure 2 also shows specific peaks related to the substrate at *m/z* 55.93 (Fe^+), 54.94 (Mn^+) and 1.00/0.44 signal ratio for 62.93/64.93 (Cu^+). Moreover, additional peaks were present that indicate the presence of alkali and alkaline earth metals on the surface, such as at *m/z* 38.96 (K^+), 22.99 (Na^+) and 39.96 (Ca^+). The Cu, K, Na and Ca are most likely due to contamination in the steel (not specified by the supplier) or in the chemicals employed. K, Na and Ca signals are usually detected in SIMS analyses due to their low ionisation energies and consequently the method's low detection limits of these species (it is possible to detect these species in the ppm range).

Figure 2b shows the negative ion SIMS spectrum obtained for the CIN surface layer adsorbed on the C15 steel in the *m/z* range of 0–200. The spectrum consists of many peaks, among which the most intensive are at *m/z* 1.01 (H^-, the base peak), 15.99 (O^-), 17.00 (OH^-), 25.01 (C_2H^-), 34.97 (Cl^-), 41.00 (C_2HO^-), 49.01 (C_4H^-), 73.01 (C_6H^-), 103.05 ($C_8H_7^-$) and 147.04 (this peak most likely corresponds to $(M–H+O)^-$). The signal for Cl arises due to the HCl medium employed to prepare the sample, and it seems that some chloride remained on the surface despite the surface being washed with ultrapure water after 1 h of immersion. The negative secondary ion mass spectrum is usually not as

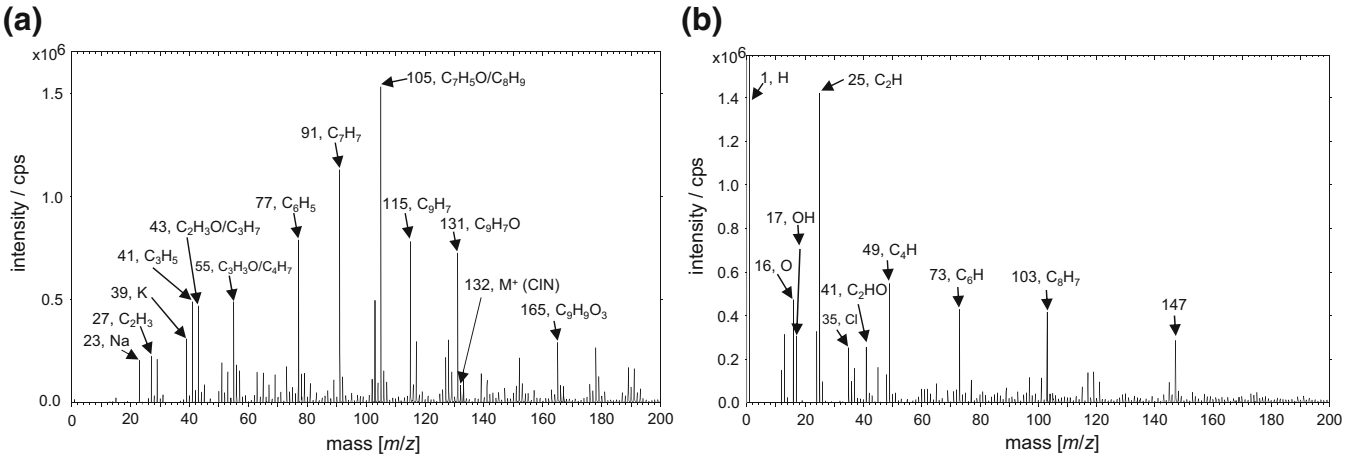

Figure 2. (**a**) The positive ion and (**b**) negative ion ToF-SIMS specta with corresponding nominal masses and suggested fragments or specific elements measured for the CIN layer adsorbed on the C15 steel

informative as the positive ion SIMS spectrum, and therefore, direct confirmation of the CIN molecule on the surface is limited with regard to the negative ion SIMS spectrum.

Chemical Structure of the PA Layer Figure 3a shows the positive ion SIMS spectrum obtained from the PA layer adsorbed on the C15 steel. The most intensive peak originates from Fe^+ at *m/z* 55.93 related to the substrate steel. The most characteristic peaks representing PA on the C15 steel surface are at *m/z* 55.02 related to the $(M–H)^+$ peak ($C_3H_3O^+$) and one at *m/z* 57.03 related to the $(M+H)^+$ peak ($C_3H_5O^+$). The PA molecular ion ($C_3H_4O^+$) has exact mass of 56.03. The inset in Figure 3a shows the narrow region around *m/z* 55, where the most characteristic $(M–H)^+$ peak ($C_3H_3O^+$) at *m/z* 55.02 is present close to the $C_4H_7^+$ peak at *m/z* 55.05. Due to the high mass resolution capability, we were able to clearly distinguish between these two peaks, thus making the SIMS method superior compared to XPS in such analysis (the XPS spectra is given below). The signal of the $(M–H)^+$ peak was used afterwards to measure additional properties such as thermal stability, as shown below. Another peak that can be related to the PA molecules occurs at *m/z* 43.02 ($C_2H_3O^+$).

In addition, as found also for CIN-treated sample, the mass spectrum in Figure 3a also shows many hydrocarbon C_xH_y-related peaks usually present on the surface, such as those at *m/z* 27.02 ($C_2H_3^+$), 29.04 ($C_2H_5^+$), 41.04 ($C_3H_5^+$), 43.09 ($C_3H_7^+$), 55.05 ($C_4H_7^+$), 57.07 ($C_4H_9^+$), 91.05 ($C_7H_7^+$) and 115.05 ($C_9H_7^+$). In addition to hydrocarbon-related peaks, signals arising from substrate-specific peaks at *m/z* 72.94 ($FeOH^+$), 127.86 (Fe_2O^+) and 144.87 ($Fe_2O_2H^+$) are also present in the positive ion SIMS mass spectrum. As also found for CIN, peaks at *m/z* 38.96 (K^+) and 22.99 (Na^+) appeared (most likely for the same reason as explained above).

Figure 3b shows the negative ion SIMS spectrum of the PA layer adsorbed on the C15 steel. The spectrum consists of many peaks, among which the most intensive are at *m/z* 1.01 (H^-, the base peak), 15.99 (O^-), 17.00 (OH^-), 25.01 (C_2H^-), 34.97 (Cl^-), 41.00 (C_2HO^-), 45.00 (CHO_2^-), 49.01 (C_4H^-), 87.92 (FeO_2^-), etc. As also reported for CIN, the measured negative secondary ion spectrum is again not as informative as a positive SIMS spectrum.

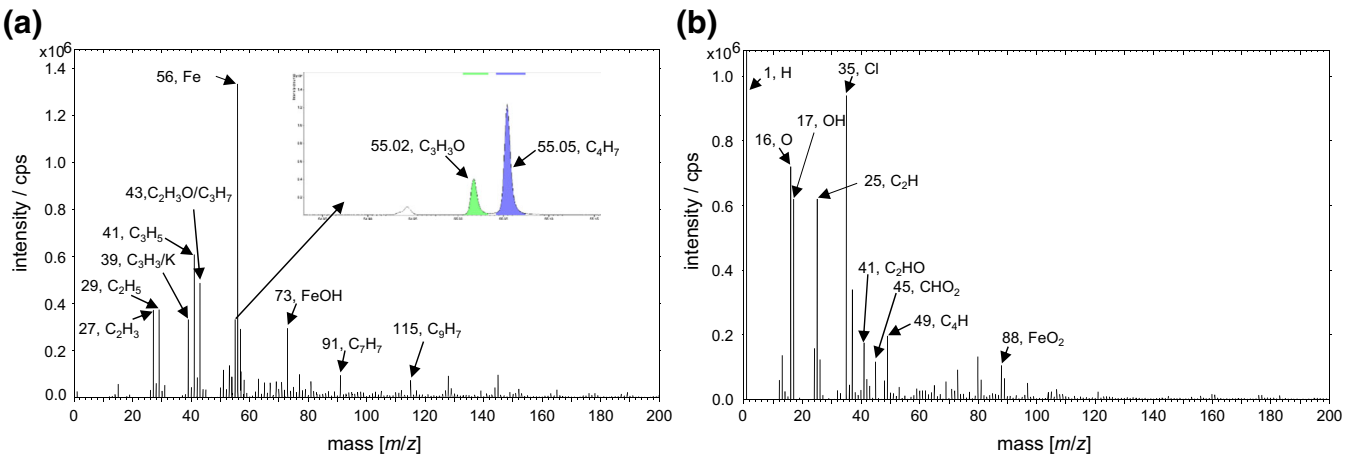

Figure 3. (**a**) The positive ion and (**b**) the negative ion ToF-SIMS spectra with corresponding nominal masses and suggested fragments or specific elements measured for the PA layer adsorbed on the C15 steel. The insert in (**a**) shows the region around *m/z* 55 where an $(M–H)^+$ peak ($C_3H_3O^+$) is present

SIMS Fragmentation Pattern It has to be noted that the fragmentation pattern is significantly different when employing SIMS compared with other MS ionisation sources, e.g. electron impact (EI), chemical ionisation or electrospray ionisation. SIMS employs the relatively strong ionisation source of accelerated ions compared with, e.g. energetically less intensive electrons when using EI. Therefore, fragments of CIN and PA obtained from other ionisation sources reported in the literature could be employed herein only informatively in order to support the relatively stable cations formed during the fragmentation procedure. Figure 4 shows suggested fragmentation reactions based on the literature using EI or electrospray ionisation [31] sources. In order to support the formed fragments, high-resolution positive ion ToF-SIMS spectra are also presented for both PA and CIN in Figure 4 (as mentioned above, only positive secondary ions are explained as are more informative compared with negative secondary ion spectrum).

The signal for the CIN parent ion is non-intensive at *m*/*z* 132.06 (also seen in Figure 2a). After CIN loses a hydrogen radical, a cinnamoyl cation at *m*/*z* 131.05 is formed [31, 32]. Further elimination of CO leads to a 2-phenylethen-1-ylium cation at *m*/*z* 103.05 [33, 34]. The CIN parent ion could also fragment forming a phenyl cation at *m*/*z* 77.04 and a benzyl cation at *m*/*z* 91.05 [34]. A known rearrangement of benzyl cation to tropylium ion is shown in Figure 4a. Furthermore, the phenyl cation fragments further to form a cyclobutadienyl cation at *m*/*z* 51.02 (Figure 4a) [34]. Additionally, in the fragmentation pattern of CIN, we suggest the formation of a 3-oxoprop-1-en-1-ylium cation at *m*/*z* 55.02 [35] and a benzoyl cation *m*/*z* 105.03 (signals for these species were measured in the high-resolution spectra, as given in Figure 4e). The known elimination of CO from benzoyl cation to give a phenyl cation to produce a signal at *m*/*z* 77.04 could also occur (as suggested in Figure 4c) [33]. All of the above-suggested fragments are supported with signals in the high-resolution spectra given in Figure 4e, where peaks are located at exact *m*/*z* corresponding to the suggested fragments.

Suggested PA fragmentation reactions are presented in Figure 4f. The parent ion peak for PA at *m*/*z* 56.03 is non-intensive (also seen in Figure 3a). The intensive peak at *m*/*z* 43.02 most likely corresponds to the vinyl cation that was formed due to the high-energetic SIMS ionisation source. When PA loses a hydrogen radical, a signal at *m*/*z* 55.02 corresponding to a 1-hydroxyprop-2-yn-1-ylium cation is formed [36]. Alternate fragmentation of propargyl alcohol leads to a prop-2-yn-1-ylium cation at *m*/*z* 39.02 and a methyleneoxonium at *m*/*z* 31.02. All of these signals were confirmed in high-resolution spectra (Figure 4g).

SIMS Imaging—the Lateral Homogeneity of the Deposited CIN Surface Layer The ToF-SIMS method also has a microscopic aspect since the primary Bi ion beam can raster over a certain analysed area. This possibility was explored herein also in the corrosion studies by investigating the spatial distribution of different signals arising from the CIN molecules and Fe-based substrate over an area of 500 × 500 μm. This analysis was performed on two different spots on the surface using both secondary ion signal modes.

Figure 5 shows optical images where the surface analysis was performed (Figure 5a, c) and the obtained mass spectra in the positive and negative modes for the signals characteristic of CIN molecules and Fe (Figure 5b, d). Figure 5b shows the signal distribution of positive secondary ions at *m*/*z* 131.05, which was shown above to be the most intensive for the parent CIN ($(M–H)^+$ in Figure 2). Moreover, simultaneously, a signal at *m*/*z* 55.93 that is characteristic of Fe^+ was also selectively analysed. Figure 5d shows the distribution of the negative secondary ions signal at *m*/*z* 43.02 ($C_2H_3O^-$, which is characteristic of CIN) and at *m*/*z* 87.92 (indicative of FeO_2^-). The negative secondary ion mode is used herein only tentatively as the signal at *m*/*z* 87.92 for the substrate C15 steel is not well expressed in Figure 2b.

The main conclusion that can be drawn from these images is that the distribution of CIN molecules on the surface is not homogeneous. It has to be pointed out that a direct correlation of CIN distribution in Figure 5b, d should not be made as two different spots on the surface were analysed for the two secondary ion modes. This analytical result of heterogeneous distribution could explain the fact that CIN, when employed as the sole corrosion inhibitor, was not as effective as PA [9, 37], because when the metallic surface is not uniformly covered by the corrosion inhibitor, it leaves some places prone to corrosion attack.

In a similar manner as for the CIN adsorbed layer, the lateral distribution of PA adsorbed molecules on the C15 steel sample was also analysed. Figure 5e shows an optical image of the analysed region and Figure 5f shows a composite chemical image obtained by positive ion signal for $C_2H_3O^+$ at *m*/*z* 43.02 (green colour), which is characteristic of PA molecules, and an FeH^+ signal (red colour) at *m*/*z* 56.94, which is characteristic of steel substrate. Based on Figure 5f, we can conclude that a more homogeneous distribution of PA molecules (green colour) over the analysed steel area is formed compared to CIN (Figure 5b, d). This also explains the fact that PA is a more effective corrosion inhibitor than CIN [9, 37]. Figure 5f shows the presence of some agglomerates rich in PA molecules of about 50 μm in diameter.

Based on the TOF-SIMS results, the adsorption of CIN and PA is confirmed. The proof of PA and CIN adsorption is more certain when using the SIMS technique (especially from the high-resolution mass spectra) compared to, e.g. XPS, from which only C–H/C–C, C–O and C=O bonds can be confirmed. The latter XPS signals can also arise from other adventitious compounds [24, 25, 29, 30], e.g. atmospheric contamination, making the XPS technique less useful for such studies (as shown below). In addition, the higher homogeneity of the PA surface layer compared with CIN was confirmed by ToF-SIMS imaging.

Furthermore, the experiments were carried out by gradually elevating the temperature and analysing these samples in order to obtain further insight into the thermal stability of the

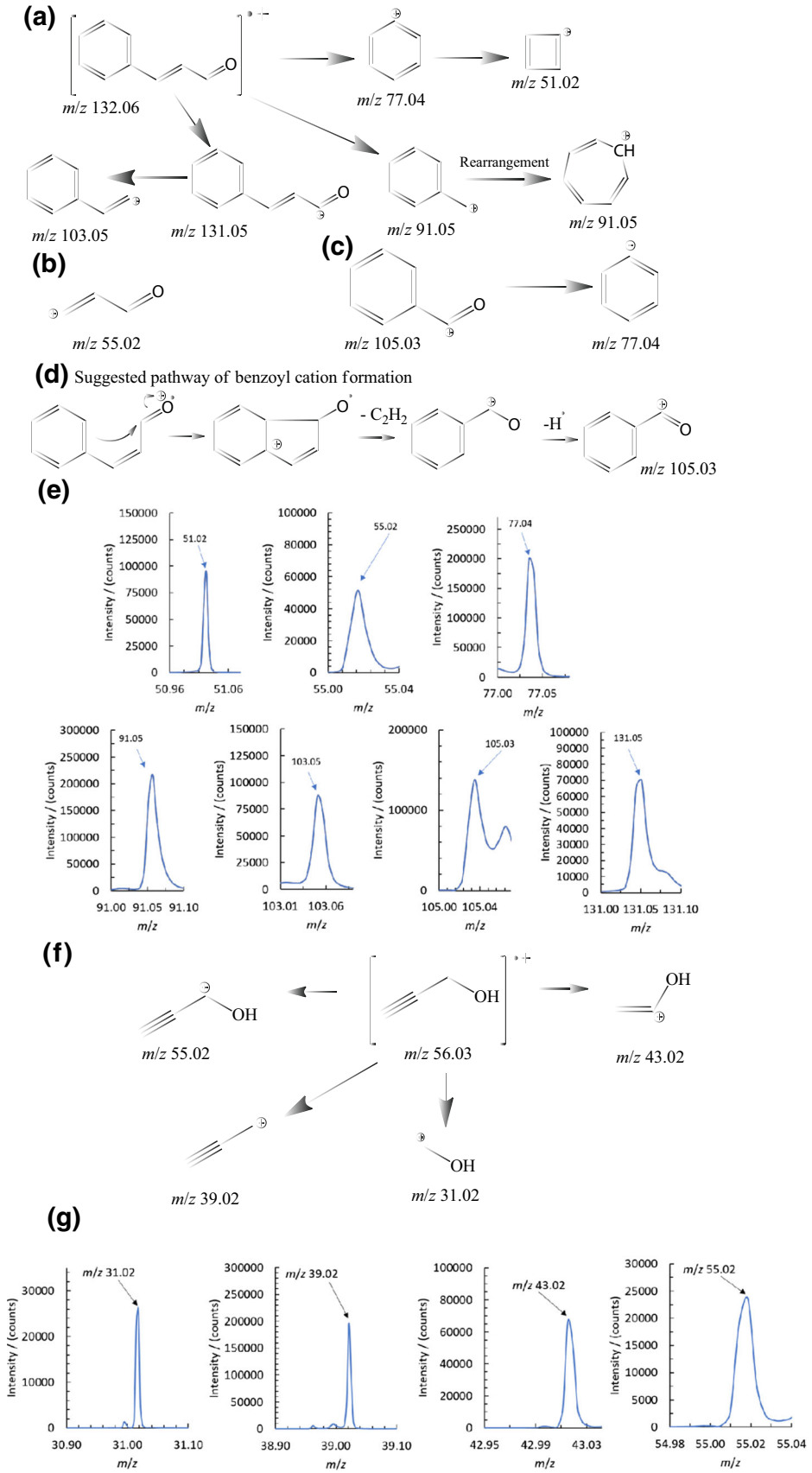

Figure 4. (**a**) Suggested CIN fragmentation, (**b**) a 3-oxoprop-1-en-1-ylium cation, (**c**) a rearrangement of benzyl cation to tropylium ion, (**d**) pathway of benzoyl cation formation, (**e**) CIN high-resolution positive-ion ToF-SIMS spectra, (**f**) suggested PA fragmentation, and (**g**) PA high-resolution positive-ion ToF-SIMS spectra

adsorbed compounds. This information is especially needed when employing such compounds, as steel materials with adsorbed corrosion inhibitors are usually exposed to elevated temperature (e.g. 150 °C and higher) [9].

Analysis of Thermal Stability by ToF-SIMS Measurements

In order to study the in situ thermal stability of the CIN layer adsorbed on the C15 steel, the sample was annealed from room temperature to 500 °C. After every annealing step, a new SIMS spectrum was measured on a fresh area close to the previously analysed area. Moving the spot analysed to a new area is necessary as the primary ion beam could sputter away a significant portion of surface atoms/molecules, which could exceed the so-called static limit (10^{13} atoms/cm^2). This might lead to a wrong interpretation of the changes in SIMS spectra not originating from thermal desorption but from extensive ion bombardment. The temperature dependence of the most characteristic peak intensities related to the CIN molecule, i.e. a peak at *m*/*z* 131.05 in the positive ion spectrum, was monitored and is presented in Figure 6a. The $(M–H)^+$ intensity at *m*/*z* 131.05 is the most important since it directly reflects the presence of CIN molecules on the surface. Some minor fluctuations around the trend curves in Figure 6a mainly originate from heterogeneous areas analysed during sample movements, as mentioned above.

Figure 6a shows that in the first annealing cycles (30–60 °C) the relative intensities of the CIN-related signal $(M–H)^+$ peak increased. We explain this by the partial desorption of some water/solvent molecules from the surface, which is then reflected as an enrichment in the density of CIN molecules in the topmost surface layer. Subsequently, the temperature dependence of the SIMS signal for the $(M–H)^+$ peak shows that the CIN layer on the C15 steel is stable up to approx. 100 °C. At higher temperature, CIN molecules start to desorb and a majority of the CIN molecules desorb up to approx. 180–200 °C. A smaller amount of CIN molecules persist on the C15 steel surface up to about 250 °C. There are some smaller variations of the curve in Figure 6a, which are related to heterogeneity of the sample surface. Namely during the annealing, the SIMS analyses were performed on fresh regions obtained by sample moving. Analysed regions most likely sometimes contain also some small inclusions and heterogeneous areas, which produced variations in the intensity curve.

Based on Figure 6a, we estimated that 150 ± 10 °C is the temperature at which the maximum desorption rate of the CIN molecules from the C15 steel was reached. This temperature was used to evaluate the desorption of the CIN molecules into a vacuum ambient assuming a first-order process, the absence of intramolecular interactions and re-adsorption as proposed by Redhead [38] and applied for a similar system by Facciotti et al. [3]. The heating rate of 5 K/min was used as a parameter for the calculation of adsorption energy according to Redhead [38]. In this way, the desorption energy of 122.5 ± 5.0 kJ/mol was calculated for the desorption of CIN molecules from steel into a vacuum ambient.

Similarly, as for the CIN corrosion inhibitor, we performed thermal desorption analyses also for the PA corrosion inhibitor. The intensities of the PA molecular signals $(M+H)^+$ at *m*/*z* 57.03 ($C_3H_5O^+$) and $(M–H)^+$ at *m*/*z* 55.02 ($C_3H_3O^+$) as a function of temperature are plotted in Figure 6b. The PA layer is stable up to about 100 °C. Further annealing in the range between 100 and 300 °C induces almost a linear decrease in the intensities of the measured signals at *m*/*z* 55.02 and 57.03. Due to the nearly linear decrease, it is difficult to determine the temperature of the maximum desorption rate, which is needed for the calculation of desorption energy in the Redhead model [38], thus making the reported value less certain. In any case, we estimated the desorption energy of PA molecules using a possible interval of the temperature of maximum desorption from 100 to 300 °C (Figure 6b). In this way, the desorption energy for the PA corrosion inhibitor from C15 steel was estimated to be in the range of 107–167 kJ/mol.

XPS Results

In order to further understand the chemistry of the CIN and PA layer adsorption on the C15 steel and to show the advantages of using the SIMS surface analytical method in corrosion studies, XPS analyses were also performed on samples prepared in the same manner. The results are given in Figure 7. Figure 7a shows the C 1s spectra with the most intensive peak located at 284.8 eV, which corresponds to C–C/C=C/C–H bonds [21–25]. In addition, for both PA- and CIN-treated C15 steel, the intensive high binding energy side shoulder in C 1s spectra indicates a C–O connection located at 286.5 eV (both compounds contain C–O bonds). The latter is more intensely expressed in the case of CIN.

A significant difference in XPS spectra can be recognised for O 1s spectra (Figure 7b). The O 1s spectrum from the PA layer consists of a peak at 530.0 eV originating from Fe-oxide under the PA layer and a peak at 531.8 eV related to the C–OH bonds in the PA molecule. For the CIN layer, three features can be distinguished: for the feature at the low binding energy side located at 530.0 eV, the signals originate from Fe-oxide, at 532.0 eV they originate from –C=O bonds and at 533.8 eV from water molecules that remained on the surface in spite of the drying procedure for the sample after immersion (the NIST Standard Reference Database reports that the O 1s signal for water appears at 532.8–538.0 eV [39]). Water molecules might be hydrogen bonded to O atoms in the PA and CIN surface layers [24, 25, 40–43].

The Fe $2p_{3/2}$ spectra for both samples are shown in Figure 7c. The most intensive component of those spectra is at 711 eV and is related to an Fe-oxide phase under the CIN or PA adsorbed layers. At the geometry where these spectra were acquired (i.e. the take-off angle of Fe 2p photoelectrons was 20°), the spectra yield very surface-sensitive information. The analysis depth in this case was approx. 2 nm and that is a reason why no peak representing a metallic Fe peak at 706 eV is present in the Fe 2p

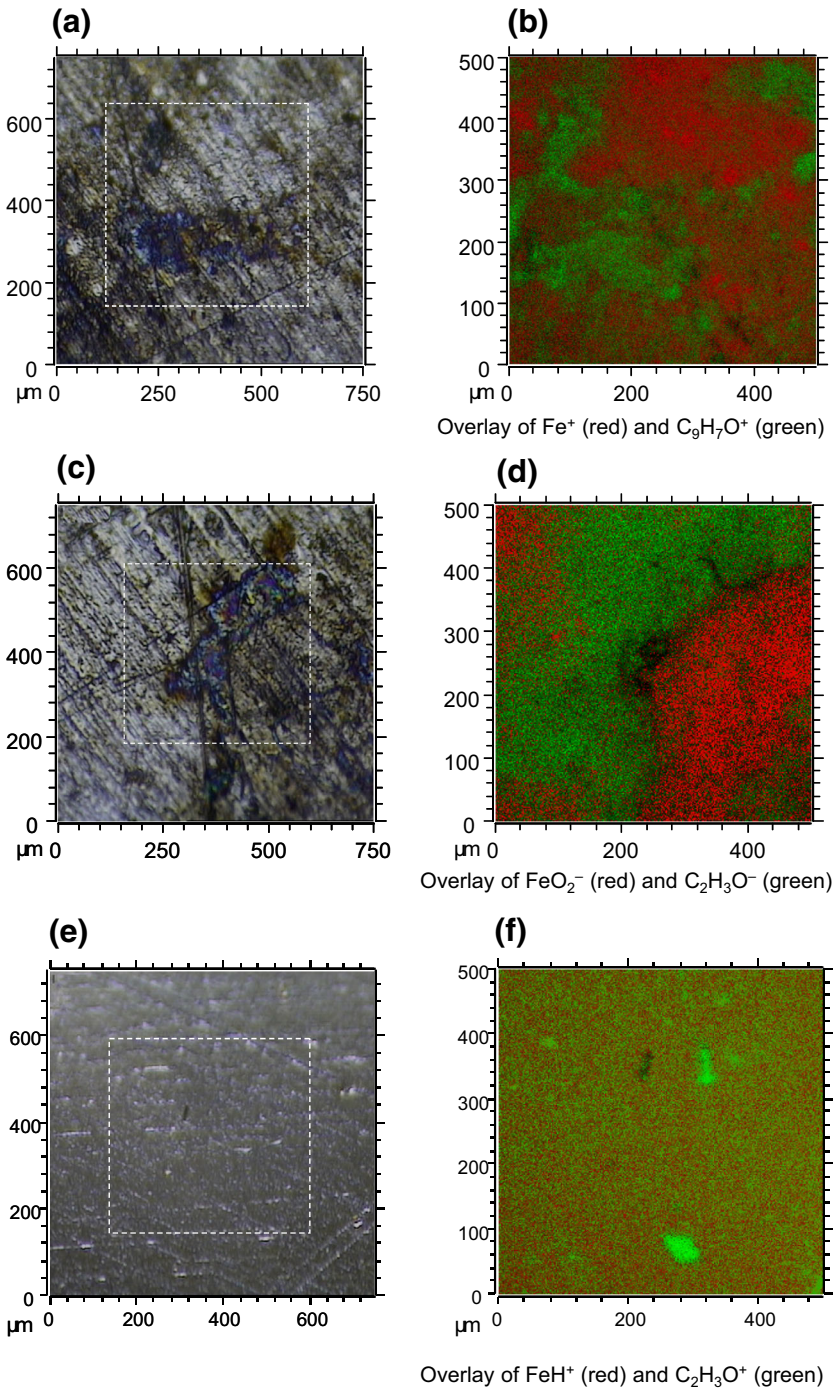

Figure 5. Optical and SIMS images of the spatial distribution of secondary ions from the CIN or PA adsorbed layer on the C15 steel: (**a**) an optical image of analysed region 1 for CIN, (**b**) a molecular specific image of the distribution of CIN molecules (the signal of positive ions at *m/z* 131.05, $C_9H_7O^+$) and of Fe^+ (*m/z* 55.93) ions over an area of 500 × 500 μm), (**c**) an optical image of analysed region 2 for CIN, (**d**) a molecular specific image of the distribution of CIN molecules (the signal of negative ions at *m/z* 43.02 ($C_2H_3O^-$) and of FeO_2^- (*m/z* 87.92) ions), (**e**) an optical image for PA, and (**f**) a molecular specific image of the distribution of PA molecules (the signal of the positive ion at *m/z* 43.02, $C_2H_3O^+$) and of FeH^+ (*m/z* 56.94) ions over an area of 500 × 500 μm

spectra. These metallic peaks were clearly visible when the take-off angle was increased, and a deeper subsurface region (about 5 nm) was probed by XPS (results not shown).

Figure 7d shows the survey XPS spectra measured on the CIN- and PA-treated samples, which shows that the ratio of C 1s to Fe 2p signals is higher for the CIN-treated sample compared with that for the PA-treated sample. This implies that more CIN molecules were adsorbed or a thicker layer was formed on the C15 steel surface compared with PA. This is also supported by the fact that the background signal is more

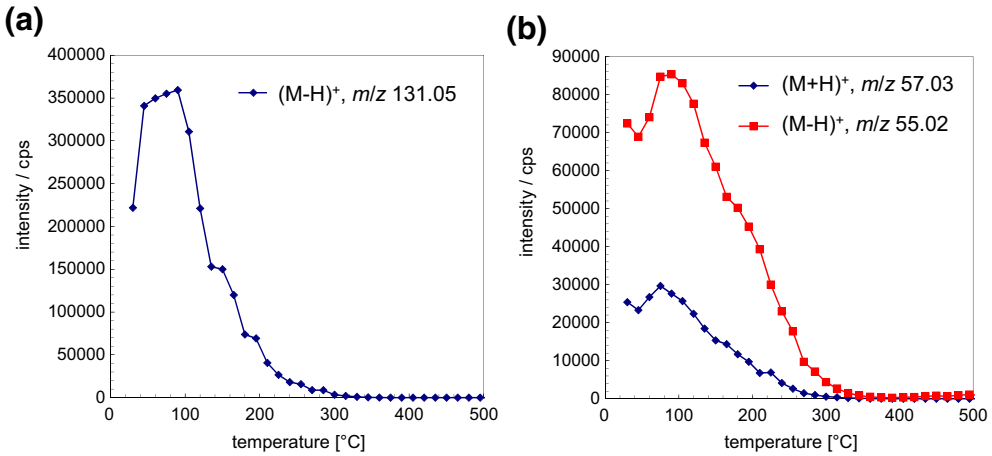

Figure 6. The temperature dependency of the positive ion SIMS signals (**a**) at *m/z* 131.05 ($C_9H_7O^+$) related to the CIN molecules and (**b**) at *m/z* 57.03 ($(M+H)^+$, $C_3H_5O^+$) and *m/z* 55.02 ($(M–H)^+$, $C_3H_3O^+$) related to the PA molecules

intensive for the CIN-treated sample in the binding energy region higher than 700 eV. This happens due to the inelastic scattering of the electrons originating from the substrate and their travelling through the adsorbed surface layers.

In summary, the XPS results confirm the successful adsorption of CIN and PA molecules and yield information confirming a higher density of CIN molecules with respect to the density of PA molecules. However, in the case of XPS compared to SIMS, one might be less certain that the C and O signals really originate from the corrosion inhibitors as also other adventitious oxygen- and carbon-containing components would show a peak at the exactly the same binding energy.

In order to monitor the thermal stability of the PA and CIN layers on the C15 steel, the thermal dependency of the carbon C 1s spectra was measured on PA- and CIN-treated samples in the temperature region between room temperature and 460 °C (for PA) and 420 °C (for CIN). The measured temperature profiles are shown in Figure 7e.

At room temperature, the carbon C 1s signal is higher for the CIN-treated sample. However, the more intensive thermal desorption (signal intensity drop) of CIN starts at 100–200 °C and reaches its minimum intensity at 390 °C. In the case of PA, the C 1s signal is relatively constant up to about 400 °C, when it starts to decrease rapidly to a minimum value at 425 °C. From this result, it can be concluded that the CIN layer is less thermally stable compared with the PA layer. The same conclusion was already given above using thermal dependency SIMS measurements.

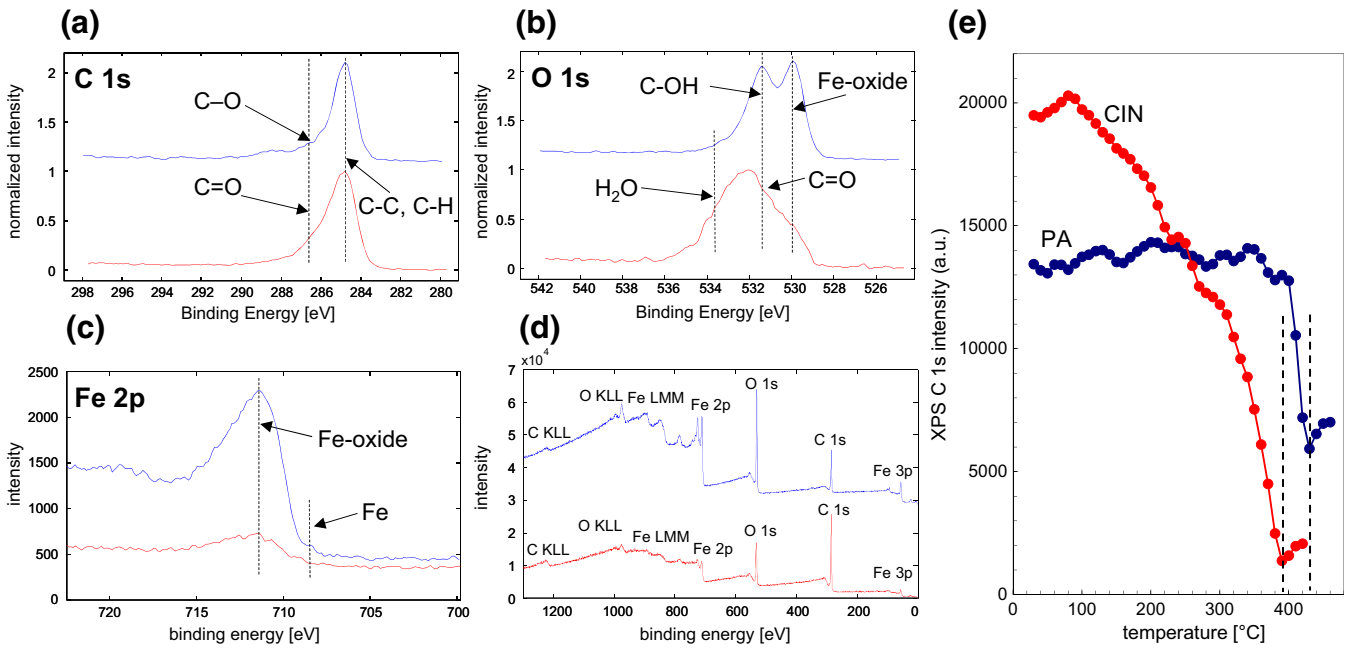

Figure 7. XPS spectra obtained on the CIN and PA layers adsorbed on the C15 steel: (**a**) C 1s spectra, (**b**) O 1s spectra, (**c**) Fe $2p_{3/2}$ spectra, (**d**) survey spectra, and (**e**) temperature dependency of the XPS intensity of the carbon C 1s spectra for the PA and CIN adsorbed layers on the C15 steel obtained during annealing from room temperature to above 400 °C. The blue spectra are from the PA layer and the red spectra from the CIN layer

The main difference between the two surface analytical methods used lies in the difference between the desorption temperatures observed with the SIMS and XPS methods. Using SIMS, a lower complete desorption temperature of adsorbed molecules was determined, i.e. for CIN at 200 °C and for PA molecules at 300 °C. One of the possible reasons may be the different chemical selectivity of both methods. With the XPS method, we can measure the total carbon C 1s signal, whereas by the SIMS method, we measured the specific molecular signal characteristics of PA and CIN molecules. It is possible that both molecules start to decompose (at 200 °C for CIN and at 300 °C for PA) and that is why their specific molecular *m/z* signals in the SIMS spectra disappeared. On the other hand, the decomposition products might remain on the surface, thus contributing to the carbon signal detected by the XPS method. The second reason might lie in the surface contamination species (adventitious carbon) that might be retained on the surface more strongly than CIN or PA molecules. Using XPS, by analysing relatively simple organic structures (as in the present case), one cannot separate the C–O arising from a corrosion inhibitor from that of oxidised adventitious carbonaceous species. The latter explains why the higher selectivity of the SIMS method compared to the XPS method gives better insight into the surface chemistry for the present case of very thin surface layers.

Imaging was also performed with the XPS method, but due to the low lateral resolution of the XPS method, it was not possible to detect heterogeneous surface distribution as was possible in the case of SIMS imaging for the CIN layer shown in Figure 5. Furthermore, by using Tougaard thickness analysis [44, 45] of the CIN and PA adsorbed surface layers on the C15 steel, the thicknesses of both layers were estimated to be thinner than 3 nm. In the present case, the same analytical procedure for the Tougaard thickness analysis was employed as reported before [21–23].

AFM Analyses

Figure 8 shows AFM micrographs obtained over 5 × 5 μm regions on the untreated steel, CIN-treated and PA-treated C15 steel. The micrograph in Figure 8a shows that the surface of the untreated C15 steel was not flat on the nanometre scale. Although the finest grounding was performed by 4000-grid SiC paper, it could not be expected that a flat surface could be obtained. This surface shows some grains of 100–200 nm in diameter (Figure 8a). After the adsorption of the CIN and PA corrosion inhibitors, the surface morphology became much flatter, indicating changes in the topmost layer. From the AFM images, the mean surface roughness was quantified to be 26 ± 3, 11 ± 3 and 8 ± 3 nm for untreated, CIN-treated and PA-treated C15 steels, respectively. The decrease in surface roughness confirms the presence of the adsorbed layer of CIN and PA corrosion inhibitors that modified the surface.

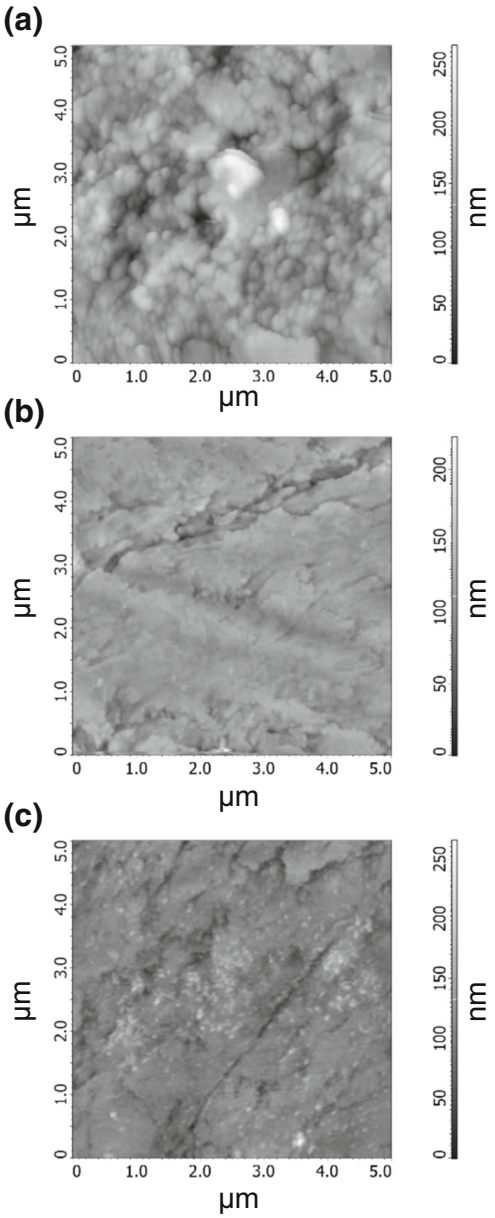

Figure 8. AFM micrographs of (**a**) C15 steel, (**b**) the CIN layer on the C15 steel and (**c**) the PA layer on the C15 steel over 5 × 5 μm large regions

Conclusions

In this work, for the first time, the positive and negative SIMS spectra were reported and explained for cinnamaldehyde (CIN) and propargyl alcohol (PA) molecules adsorbed on steel surface. In the analysis of CIN corrosion inhibitor molecules, an $(M–H)^+$ signal was identified at *m/z* 131.05, corresponding to $C_9H_7O^+$ in the positive ion SIMS spectra. The adsorption of PA molecules was also confirmed by a $(M–H)^+$ signal at *m/z* 55.02 ($C_3H_3O^+$) in the positive SIMS spectrum. The latter was also supported by the high-resolution SIMS mass spectrum in order to selectively separate this signal from the possible carbon-containing adventitious species on the surface. The direct evidence of the adsorption of CIN and PA molecules was possible due to the low

detection limit and selectivity of the ToF-SIMS method, even for very thin layers (in the nm range), as shown in this study. On the other hand, the negative ion SIMS spectra for the same system were less useful in confirming the adsorption of these compounds. Moreover, such a confident confirmation of these species on the steel surface was not possible with the XPS method.

The possibility of spatially resolved ToF-SIMS analyses with high mass resolution allowed us to follow the lateral distribution of the adsorbed corrosion inhibitors. In this way, we identified the non-homogenous distribution of CIN molecules on the C15 steel surface. On the other hand, in the case of PA, a more homogenous distribution of PA molecules on the C15 steel surface with some PA agglomerates was detected. Moreover, for such thin surface layers in the nanometre range, imaging was possible only in the case of SIMS and not with XPS in order to reveal the surface distribution of the CIN or PA molecules due to the selective signal that is obtained with SIMS and that can be separated from that for the other adventitious species on the surface. The latter was not possible with the XPS method for the same system.

Using SIMS, it was also possible to show the temperature stability of the corrosion inhibitors by annealing the samples in a vacuum ambient and performing an in situ ToF-SIMS analysis. We estimated the desorption temperature for the CIN corrosion inhibitor to be 150 ± 10 °C, from which the desorption energy for the CIN layer on the C15 steel was calculated to be 122 ± 5 kJ/mol. For the PA corrosion inhibitor, desorption from C15 steel occurs over a wider temperature range between 100 and 300 °C, which allowed us to estimate the desorption energy for the PA corrosion inhibitor to be in the range of 107–167 kJ/mol. It was also shown that due to the higher selectivity of the SIMS method compared to the XPS method, the desorption temperatures reported are more certain.

To conclude, in the present case, the SIMS method proved to be more useful compared to XPS for the surface analysis of CIN and PA molecules adsorbed on steel surface.

Acknowledgments

The authors wish to gratefully thank Dr. Gregor Jakša and Tatjana Filipič for their help with ToF-SIMS and XPS measurements. The financial support from the Slovenian Research Agency is also greatly appreciated (Grant Numbers P2-0032, P2-0082, and J1-9169).

References

1. Friedbacher, G., Bubert, H.: Surface and Thin Film Analysis: a Compendium of Principles, Instrumentation, and Applications, 2nd edn. Wiley-VCH, Weinheim (2011)
2. Coelho, L.B., Cossement, D., Olivier, M.G.: Benzotriazole and cerium chloride as corrosion inhibitors for AA2024-T3: an EIS investigation supported by SVET and ToF-SIMS analysis. Corros. Sci. **130**, 177–189 (2018)
3. Facciotti, M., Amaro, P.S., Brown, R.C.D., Lewin, P.L., Pilgrim, J.A., Wilson, G., Jarman, P.N., Fletcher, I.W.: Static secondary ion mass spectrometry investigation of corrosion inhibitor Irgamet®39 on copper surfaces treated in power transformer insulating oil. Corros. Sci. **98**, 450–456 (2015)
4. Brundle, C.R., Grunze, M., Mäder, U., Blank, N.: Detection and characterization of dimethylethanolamine-based corrosion inhibitors at steel surfaces. I. The use of XPS and ToF-SIMS. Surf. Interface Anal. **24**, 549–563 (1996)
5. Diwan, A., Singh, B., Hurley, C.J., Linford, M.R.: Layer-by-layer deposition of nitrilotris(methylene)triphosphonic acid and Zr(IV): an XPS, ToF-SIMS, ellipsometry, and AFM study. Surf. Interface Anal. **48**, 105–110 (2016)
6. Madaan, N., Diwan, A., Linford, M.R.: Fluorine plasma treatment of bare and nitrilotris(methylene)triphosphonic acid (NP) protected aluminum: an XPS and ToF-SIMS study. Surf. Interface Anal. **47**, 56–62 (2015)
7. Sastri, V.S.: Green Corrosion Inhibitors: Theory and Practice, John Wiley & Sons, Hoboken (2011)
8. Frail, P.R., Zorn, G., Morra, M.M.: Performance Analysis of Commercial Azoles for Yellow Metal Corrosion Control Utilizing Surface Analysis and Electrochemistry, NACE - International Corrosion Conference Series (2014)
9. Finšgar, M., Jackson, J.: Steel corrosion and the application of corrosion inhibitors in acidic media for the oil and gas industry: a review. Corros. Sci. **86**, 17–41 (2014)
10. Jayaperumal, D.: Effects of alcohol-based inhibitors on corrosion of mild steel in hydrochloric acid. Mater. Chem. Phys. **119**, 478–484 (2010)
11. Quraishi, M.A., Jamal, D.: Corrosion inhibition of N-80 steel and mild steel in 15% boiling hydrochloric acid by a triazole compound—SAHMT. Mater. Chem. Phys. **68**, 283–287 (2001)
12. Gao, J., Weng, Y., Salitanate, S., Feng, L., Yue, H.: Corrosion inhibition of α,β-unsaturated carbonyl compounds on steel in acid medium. Pet. Sci. **6**, 201–207 (2009)
13. Sastri, V.S.: Corrosion Inhibitors: Principles and Applications, p. 747. Wiley, Chichester (2001)
14. Walker, M.L.: Method and composition for acidizing subterranean formations. US Patent 4,498,997 (1985)
15. Baddini, A.L.d.Q., Cardoso, S.P., Hollauer, E., Gomes, J.A.d.C.P.: Statistical analysis of a corrosion inhibitor family on three steel surfaces (duplex, super-13 and carbon) in hydrochloric acid solutions. Electrochim. Acta. **53**, 434–446 (2007)
16. Barmatov, E., Geddes, J., Hughes, T., Nagl, M.: Research on corrosion inhibitors for acid stimulation. NACE. C2012–C0001573 (2012)
17. Nasr-El-Din, H.A., Al-Othman, A.M., Taylor, K.C., Al-Ghamdi, A.H.: Surface tension of HCl-based stimulation fluids at high temperatures. J. Pet. Sci. Eng. **43**, 57–73 (2004)
18. Singh, D.D.N., Dey, A.K.: Synergistic effects of inorganic and organic cations on inhibitive performance of propargyl alcohol on steel dissolution in boiling hydrochloric acid solution. Corrosion. **49**, 594–600 (1993)
19. Hill, D.G., Romijn, H.: Reduction of risk to the marine environment from oilfield chemicals: environmentally improved acid corrosion inhibition for well stimulation, corrosion. Paper No. 00342, 1–20 (2000)
20. Finšgar, M., Milošev, I.: Corrosion study of copper in the presence of benzotriazole and its hydroxy derivative. Mater. Corros. **62**, 956–966 (2011)
21. Finšgar, M.: 2-Mercaptobenzimidazole as a copper corrosion inhibitor: part II. Surface analysis using X-ray photoelectron spectroscopy. Corros. Sci. **72**, 90–98 (2013)
22. Finšgar, M.: EQCM and XPS analysis of 1,2,4-triazole and 3-amino-1,2,4-triazole as copper corrosion inhibitors in chloride solution. Corros. Sci. **77**, 350–359 (2013)
23. Finšgar, M., Kek Merl, D.: 2-Mercaptobenzoxazole as a copper corrosion inhibitor in chloride solution: electrochemistry, 3D-profilometry, and XPS surface analysis. Corros. Sci. **80**, 82–95 (2013)
24. Finšgar, M., Fassbender, S., Hirth, S., Milošev, I.: Electrochemical and XPS study of polyethyleneimines of different molecular sizes as corrosion inhibitors for AISI 430 stainless steel in near-neutral chloride media. Mater. Chem. Phys. **116**, 198–206 (2009)
25. Finšgar, M., Fassbender, S., Nicolini, F., Milošev, I.: Polyethyleneimine as a corrosion inhibitor for ASTM 420 stainless steel in near-neutral saline media. Corros. Sci. **51**, 525–533 (2009)
26. N.C.W. National Institute of Standards and Technology, SRD 69
27. Popczun, N.J., Breuer, L., Wucher, A., Winograd, N.: Ionization probability in molecular secondary ion mass spectrometry: protonation efficiency of sputtered guanine molecules studied by laser postionization. J. Phys. Chem. C. **121**, 8931–8937 (2017)

28. Conlan, X.A., Baker, M.J., Krieg, R., Lockyer, N.P., Vickerman, J.C., Barnett, N.W., Lim, K.F.: Insight into the swelling mechanism involved in the recovery of serial numbers erased from polymer surfaces. Surf. Interface Anal. **43**, 625–627 (2011)
29. Finšgar, M., Kovač, J., Milošev, I.: Surface analysis of 1-hydroxybenzotriazole and benzotriazole adsorbed on Cu by X-ray photoelectron spectroscopy. J. Electrochem. Soc. **157**, C52–C60 (2010)
30. Finšgar, M.: 2-Mercaptobenzimidazole as a copper corrosion inhibitor: part I. Long-term immersion, 3D-profilometry, and electrochemistry. Corros. Sci. **72**, 82–89 (2013)
31. Cheng, G., Nan, H., Kezhi, J., Weixiang, C., Xiaoxia, W., Yuanjiang, P.: Study of fragmentation pathways of lithiated α,β-unsaturated thioesters by electrospray ionization mass spectrometry. Rapid Commun. Mass Spectrom. **24**, 409–414 (2010)
32. Hu, N., Tu, Y.-P., Liu, Y., Jiang, K., Pan, Y.: Dissociative protonation and proton transfers: fragmentation of α,β-unsaturated aromatic ketones in mass spectrometry. The Journal of Organic Chemistry. **73**, 3369–3376 (2008)
33. Silverstein, R.M., Webster, F.X.: Spectrometric identification of organic compounds, 8th edn. Wiley (2014)
34. Gross, J.H.: Mass Spectrometry, 2nd edn, (2011)
35. Abbasi, M.A., Anwar, A., Rehman, A., Siddiqui, S.Z., Rubab, K., Shah, S.A.A., Lodhi, M.A., Khan, F.A., Ashraf, M., Alam, U.: Synthesis, enzyme inhibition and molecular docking studies of 1-arylsulfonyl-4-phenylpiperazine derivatives. Pak. J. Pharm. Sci. **30**, 1715–1724 (2017)
36. Holmes, J.L., Terlouw, J.K., Burgers, P.C.: [C3H3O]+ ions; reacting and non-reacting configurations. Org. Mass Spectrom. **15**, 140–143 (1980)
37. Finšgar, M., Jackson, J.: Electrochemical study of AISI C1018 steel in methanesulfonic acid containing an acetylenic alcohol-based corrosion inhibitor formulation. J. Lab. Autom. **21**, 632–641 (2016)
38. Redhead, P.A.: Thermal desorption of gases. Vacuum. **12**, 203–211 (1962)
39. Naumkin, A.V., Kraut-Vass, A., Gaarenstroom, S.W., Powell, C.J.: NIST Standard Reference Database 20, Version 4.1 (web version), (http://srdata.nist.gov/xps/) (2003)
40. Chadwick, D., Hashemi, T.: Electron spectroscopy of corrosion inhibitors: surface films formed by 2-mercaptobenzothiazole and 2-mercaptobenzimidazole on copper. Surf. Sci. **89**, 649–659 (1979)
41. Fonder, G., Laffineur, F., Delhalle, J., Mekhalif, Z.: Alkanethiol-oxidized copper interface: the critical influence of concentration. J. Colloid Interface Sci. **326**, 333–338 (2008)
42. Chadwick, D., Hashemi, T.: Benzotriazole adsorption on copper studied by X-ray photoelectron spectroscopy. J. Electron Spectrosc. Relat. Phenom. **10**, 79–83 (1977)
43. Duret-Thual, C., Costa, D., Yang, W.P., Marcus, P.: The role of thiosulfates in the pitting corrosion of Fe-17Cr alloys in neutral chloride solution: electrochemical and XPS study. Corros. Sci. **39**, 913–933 (1997)
44. Tougaard, S.: Quantification of nano-structures by electron spectroscopy in surface analysis by auger and X-ray photoelectron spectroscopy. In: Briggs, D., Grant, J.T. (eds.) Surface Spectra, pp. 295–343. IM Publications, Manchester (2003)
45. Tougaard, S.: Surface nanostructure determination by x-ray photoemis-807 sion spectroscopy peak shape analysis. J. Vac. Sci. Technol. **14**, 1415–1423 (1996)